

# First and Second Sound Modes of a Bose-Einstein Condensate in a Harmonic Trap

V.B. Shenoy and Tin-Lun Ho

*Department of Physics, The Ohio State University, Columbus, Ohio 43210*

(December 2, 2024)

## Abstract

We have calculated the first and second sound modes of a dilute interacting Bose gas in a spherical trap for temperatures ( $0.6 < T/T_c < 1.2$ ) and for systems with  $10^4$  to  $10^8$  particles. The second sound modes (which exist only below  $T_c$ ) generally have a stronger temperature dependence than the first sound modes. The puzzling temperature variations of the sound modes near  $T_c$  recently observed at JILA in systems with  $10^3$  particles match surprisingly well with those of the first and second sound modes of much larger systems.

Since the discovery of Bose-Einstein condensation in atomic gases of alkali atoms [1], many experimental and theoretical studies have focused on the spatial structure and the collective excitations of these systems. At the same time, there has been great interest in finding ways to probe the broken gauge symmetry (*i.e.*, the “phase”) of the condensate. At present, the spatial structure of the system is well explained by the simple mean field theory [2]. The collective modes measured at very low temperatures [3] are also in agreement with theoretical predictions [4]. The major features that remain to be explained are the temperature dependence and the dissipation of the sound modes above  $0.5T_c$  recently observed by Jin et.al at JILA [5]. Jin et.al have speculated that the “ $m = 0$ ” mode that they observed could be the so-called “second sound” mode. If this were true, it would be a demonstration of the broken gauge symmetry of the system, since as Landau pointed out long ago, the second sound mode is a direct consequence of such a broken symmetry. However, in the absence of a detailed calculation consistent with experiments, the identification of the second sound mode would be difficult.

To help identify the nature of the sound modes, we have solved the linearized two-fluid hydrodynamic equations of an interacting dilute Bose gas in a spherical harmonic trap. We have in mind systems that are sufficiently large so that the hydrodynamic approach is accurate [6]. Our goal is to work out the hydrodynamic modes of this simple system as completely as possible so that it can be used as a reference for future experiments and theoretical studies. It should be noted that the recent experiments at JILA [5] were performed on small systems with a few thousand atoms. While the hydrodynamic modes of a large system may be different from the sound modes of a small one, the study of the former is important in its own right. After all, the number of atoms in the Bose condensate has increased from  $10^3$  to  $10^6$  within six months after the initial discovery [1]. It would not be surprising if Bose condensates with  $10^9$  atoms were produced in the near future. On the other hand, the hydrodynamic modes of a large system *are* relevant for the sound modes of small systems,

as the former must evolve smoothly into the latter as the number of trapped atoms is decreased continuously. This suggests the possibility of identifying the nature of sound modes of a small system by studying their hydrodynamic counterparts in a large one. Indeed, comparing our results (for systems with  $10^4$  to  $10^8$  atoms) with the JILA observations [5], we find that the temperature variations of the observed sound modes show up in the analogous modes of the larger systems in a spherical trap. In particular, the “mysterious” behaviors of the JILA ( $m = 0$ ) and ( $m = 2$ ) modes [5] in the range  $0.5 < T/T_{co} < 0.8$  match closely with the behaviors of the second sound modes of the larger systems in same temperature range, while the frequency and temperature dependence of the observed ( $m = 0$ ) mode above  $T_c$  are identical to those of the first sound mode in the same temperature range. (The temperatures  $T_{co}$  and  $T_c$  are the transition temperature for the ideal Bose and the dilute interacting Bose gas respectively). Detailed discussions on these comparisons will be given later.

Our choice of spherical symmetry is to keep the calculations manageable. Even for this simple geometry, sorting out all the hydrodynamic modes remains nontrivial. To simplify further, and as a first step, we shall ignore dissipation. While it is entirely feasible within our scheme to include dissipative effects, we feel that it is important (as in bulk  $^4\text{He}$ ) to first understand dissipationless hydrodynamics, so that one can clearly identify the dissipative effects later in a complete solution. We have calculated essentially “all” the observable first and second sound modes for  $T > 0.6T_c$ , which covers most of the temperature range of the JILA experiment [5]. The first and second sound modes are labelled by pairs of quantum numbers  $(\ell, n_1)$  and  $(\ell, n_2)$  respectively, where  $\ell$  is the angular momentum and  $n_i$  is the number of nodes in the radial direction. Our solutions show that the first sound modes are *in phase* pressure and temperature oscillations which extend over the entire cloud (spanning both the condensate and the non-condensate regions). Their frequencies vary only weakly with temperature. On the other hand, the second sound modes are *out of phase* pressure and temperature oscillations which are more and more confined in the condensate region as  $T \rightarrow T_c$ . Their frequencies vary strongly with temperature.

**Linearized Hydrodynamics :** We begin with the two-fluid hydrodynamic equations of Bosons with mass  $M$  in an external potential [7],  $M\dot{\mathbf{n}} = -\nabla \cdot \mathbf{g}$ ,  $\dot{g}_i = -n\nabla_i\phi - \nabla_j\Pi_{ij}$ ,  $\dot{s} = -\nabla \cdot (s\mathbf{v}_n)$ , and  $\dot{\mathbf{v}}_s = -\frac{1}{M}\nabla(\mu + \phi + M\mathbf{v}_n \cdot \mathbf{v}_s)$ , where  $n$ ,  $\mathbf{g}$ ,  $\Pi_{ij}$ ,  $s$ ,  $\mu$  are the number density, the momentum density, the stress tensor, the entropy density, and the chemical potential respectively. Here,  $\mathbf{v}_n$  and  $\mathbf{v}_s \equiv (\hbar/M)\nabla\theta$  are the normal fluid and superfluid velocities respectively, where  $\theta$  is the phase of condensate. The potential energy,  $\phi(r)$ , assumes the form,  $\phi(r) = \frac{1}{2}M\omega_T^2 r^2$ , for a spherical harmonic trap with frequency  $\omega_T$ . In the presence of a condensate,  $n$ ,  $\mathbf{g}$ , and  $\Pi_{ij}$  are of the form  $n = n_s + n_n$ ,  $\mathbf{g} = M(n_n\mathbf{v}_n + n_s\mathbf{v}_s)$ , and  $\Pi_{ij} = P\delta_{ij} + M(n_nv_{ni}v_{nj} + n_sv_{si}v_{sj})$ , where  $n_s$  and  $n_n$  are the superfluid and normal fluid number densities, and  $P$  is the pressure. Denoting the equilibrium quantities by the subscript “ $o$ ”, we have

$$\mathbf{v}_{no} = \mathbf{v}_{so} = 0, \quad \nabla P_o + n_o \nabla \phi = 0, \quad \nabla(\mu_o + \phi) = 0. \quad (1)$$

Making use of the well known Gibbs-Duhem relation  $d\mu = -\sigma dT + dP/n$ , where  $\sigma \equiv s/n$  is the entropy per particle, Eq.(1) leads to the expected condition of uniform temperature *ie.*,  $\nabla T_o = 0$ . Because of the external potential, the equilibrium particle and entropy densities vary as

$$\nabla n_o = \left( \frac{\partial n}{\partial P} \right)_{T_o} \nabla P_o = -n_o \left( \frac{\partial n}{\partial P} \right)_{T_o} \nabla \phi, \quad \nabla \sigma_o = \left( \frac{\partial \sigma_o}{\partial P} \right)_{T_o} \nabla P_o = -\frac{1}{n_o} \left( \frac{\partial n}{\partial T} \right)_{P_o} \nabla \phi, \quad (2)$$

where we have made use of the Maxwell relation  $(\partial \sigma / \partial P)_T = n^{-2} (\partial n / \partial T)_P$ .

Denoting the deviation of any quantity  $x$  from its equilibrium value  $x_o$  as  $\delta x \equiv x - x_o$ , the hydrodynamic equations can be linearized about the equilibrium solution and written as

$$\text{I: } \delta \dot{n} = -\nabla \cdot (n_o \mathbf{v}_s + n_{no} \mathbf{w}), \quad \text{II: } n_o \dot{\mathbf{v}}_s + n_{no} \dot{\mathbf{w}} = -(\delta n \nabla \phi + \nabla \delta P) / M \quad (3)$$

$$\text{III: } \dot{\mathbf{v}}_s = \frac{1}{M} \nabla \left( \sigma_o \delta T - \frac{\delta P}{n_o} \right), \quad \text{IV: } \delta \dot{s} = -\nabla \cdot (s_o \mathbf{v}_n), \quad (4)$$

where  $\mathbf{w} = \mathbf{v}_n - \mathbf{v}_s$ . Using eq.(2), **I** and **II** imply that

$$M \delta \ddot{n} = \nabla \cdot \left[ n_o \nabla \left( \frac{\delta P}{n_o} \right) - \delta T n_o \nabla \sigma_o \right] \equiv A. \quad (5)$$

Again using eq.(2), we have from **II** and **III**

$$\dot{\mathbf{w}} = -\frac{n_o \sigma_o}{M n_{no}} \nabla \delta T, \quad (6)$$

which implies  $M \dot{\mathbf{v}}_n = M(\dot{\mathbf{v}}_s + \dot{\mathbf{w}}) = \nabla \left( \sigma_o \delta T - \frac{\delta P}{n_o} \right) - \frac{n_o \sigma_o}{n_{no}} \nabla \delta T$ . By noting that  $\dot{s} = \sigma_o \dot{n} + n_o \dot{\sigma}$ , **IV** implies  $\dot{\sigma} = -\dot{\mathbf{v}}_n \cdot \nabla \sigma_o - \frac{\sigma_o}{n_o} \nabla \cdot (n_{so} \dot{\mathbf{w}})$ , hence

$$M \ddot{\sigma} = -(\nabla \sigma_o)^2 \delta T + \frac{1}{n_o} \nabla \cdot \left( \frac{n_o n_{so} \sigma_o^2}{n_{no}} \nabla \delta T \right) + \nabla \sigma_o \cdot \nabla \left( \frac{\delta P}{n_o} \right) \equiv B. \quad (7)$$

Expressing all quantities in terms of  $\delta T$  and  $\delta P$ , Eqs.(5) and (7) form a closed set :  $(\frac{\partial n}{\partial P})_T \delta \ddot{P} + (\frac{\partial n}{\partial T})_P \delta \ddot{T} = A/M$ ,  $(\frac{\partial \sigma}{\partial P})_T \delta \ddot{P} + (\frac{\partial \sigma}{\partial T})_P \delta \ddot{T} = B/M$ . Again, making use of the Maxwell relation  $(\partial \sigma / \partial P)_T = n^{-2} (\partial n / \partial T)_P$ , these equations can be written as

$$M \begin{pmatrix} \delta \ddot{P} \\ \delta \ddot{T} \end{pmatrix} = \begin{pmatrix} (\partial P / \partial n)_\sigma & n^2 (\partial T / \partial n)_\sigma \\ (\partial T / \partial n)_\sigma & T / c_v \end{pmatrix}_o \begin{pmatrix} A \\ B \end{pmatrix}, \quad (8)$$

where  $c_v = T(\partial \sigma / \partial T)_n$  is the specific heat per particle. The solutions of Eq.(8) are the hydrodynamic modes of the system. Since  $(\partial T / \partial n)_\sigma = -T c_v^{-1} (\partial \sigma / \partial n)_T$  and  $(\partial P / \partial n)_\sigma = (\partial P / \partial n)_T + (\partial P / \partial T)_n (\partial T / \partial n)_\sigma$ , we only need to evaluate  $n_o$ ,  $n_{so}$ ,  $n_{no}$ ,  $\sigma_o$ ,  $c_{vo}$ ,  $(\partial \sigma / \partial n)_{T_o}$ , and  $(\partial P / \partial n)_{T_o}$  to find all the coefficients in Eq.(8).

**Thermodynamics :** The thermodynamics of a trapped dilute Bose gas has been worked out within the local density approximation (LDA) by Chou, Yang and Yu (CYY) [8]. As pointed out by CYY, LDA is valid if (a)  $\epsilon \equiv \hbar \omega / k_B T \ll 1$ , and (b)  $\lambda \gg a$ , where  $\lambda \equiv \sqrt{2\pi \hbar^2 / M k_B T}$  is the thermal wavelength and  $a$  is the s-wave scattering length. Although these conditions automatically exclude very low and very high temperature limits, they are

satisfied over a very wide range of temperatures above and below  $T_c$  for large clouds. As discussed in CYY, LDA describes the physics over scales greater than  $a_T \equiv \sqrt{\hbar/M\omega_T}$ , and *all structures on the scale of  $a_T$  and smaller are shrunk to a point*. Since the typical width of the interface between the condensate and the surrounding normal gas is less than  $a_T$  [9], it is treated as a surface of zero thickness (say, at  $r = r^*$ ) within this scheme. The density is continuous at  $r^*$  but its slope is not [8]. This also causes discontinuities in a number of other quantities in Eq.(8). Because of these discontinuities, it is necessary to find the boundary conditions to relate the solutions in the regions inside and outside the surface  $r = r^*$ . The identification of these boundary conditions is the key to our numerical approach, and will be addressed in the discussions on *Numerical Methods* to follow.

Further simplification can be made within the temperature range  $a\lambda^2 n_o \ll 1$  (denoted as condition (c)), where all thermodynamic quantities can be worked out analytically. Condition (c) is generally more restrictive than (a) above. However, it still covers a wide range of temperatures. For a gas of  $^{87}\text{Rb}$  with  $N \sim 10^6$  in a trap with  $\omega_T \sim 10^3 \text{sec}^{-1}$ , the condition (c) is satisfied over the range  $0.6 < T/T_c < 1.2$  that we studied. The coefficients in eq.(8) can be calculated in a straightforward manner from the results of CYY [8] and the classic work of Lee and Yang [10]. We shall not present the details here for length reasons. Instead, we outline the procedure and give the final expressions :

- (i) Let  $T_o$  be the equilibrium temperature and  $T_c$  be the critical temperature for Bose condensation. To determine the density profile below  $T_c$ , *i.e.*, when  $T_o < T_c$ , we first specify the chemical potential  $\mu_o$  (which is uniquely determined by  $N$  as explained later). This immediately determines the size of the condensate droplet  $r^*$  through the relation  $\mu_o = \phi(r^*) + 2gn_c(T_o)$ , where  $n_c(T) \equiv \lambda^{-3}g_{3/2}(1)$ .
- (ii) The region  $r < r^*$  consists of both the condensate and the normal components, with  $n_{no}(r) = n_c(T_o)$ , and  $n_{so}(r) = g^{-1}[\phi(r^*) - \phi(r)]$ . The region  $r > r^*$  consists of only the normal component, with  $n_o(\mathbf{r})$  determined self consistently from the relation  $n(\mathbf{r}) = \lambda^{-3}g_{3/2}(\zeta(\mathbf{r}))$ , where  $\ln\zeta(\mathbf{r}) = \beta[\mu_o - \phi(r) - 2gn_o(\mathbf{r})]$ . The quantities  $N$  and  $\mu_o$  are related through the constraint that the density when integrated over all space should yield the total number of trapped atoms, *i.e.*,  $N = 4\pi \int dr r^2 [n_{so}(r) + n_{no}(r)]$ . This relation combined with the condition  $\mu_o = 2gn_c(T_c)$  gives  $T_c$  as a function of  $N$ .
- (iii) When  $a\lambda^2 n_o \ll 1$ , the Hemholtz free energy in the superfluid and normal regions are

$$f(n(\mathbf{r}), T) = -k_B T \lambda^{-3} g_{5/2}(1) + (g/2)[n(\mathbf{r})^2 + 2n(\mathbf{r})n_c(T) - n_c(T)^2], \quad r < r^*, \quad (9)$$

and

$$f(n(\mathbf{r}), T) = -k_B T \lambda^{-3} g_{5/2}(\zeta(\mathbf{r})) + k_B T n(\mathbf{r}) \ln \zeta(\mathbf{r}) + gn(\mathbf{r})^2, \quad r > r^*, \quad (10)$$

respectively. From these two equations, it is straightforward to calculate all the thermodynamic quantities needed in Eq.(8): for example,  $P = -f + n(\partial f / \partial n)_T$  and  $\sigma = s/n = -n^{-1}(\partial f / \partial T)_n$ , and so forth.

**Numerical Method :** Since Eq.(5) and (7) are smooth inside and outside  $r^*$ , it can be solved in each of these regions in a standard way by discretizing it on a grid which is made finer as  $r \rightarrow r^*$ . Because some coefficients of these equations are discontinuous at  $r^*$ , (as explained before), the solution of these equations must be understood mathematically in terms of the following limiting process. Firstly, we note that the hydrodynamic equations

**I** to **IV** are independent of the specific form of the free energy  $f(T, n)$ . We can then imagine solving these equations for a family of free energies  $f(T, n; \tau)$  parametrized by a variable  $\tau$ , which changes from the true free energy  $f^{\text{true}}$  to the LDA free energy  $f^{\text{LDA}}$  in a smooth manner as  $\tau$ , say, varies from 0 to 1. Such a change, of course, amounts to gradually collapsing the actual interface into a very thin region centered at  $r^*$ . During the process of collapse,  $\delta P$  and  $\delta T$  are smooth everywhere. The most rapid changes takes place at the boundary of the interface (which we denote as  $r^* \pm \Delta$ ), while  $\delta P$  and  $\delta T$  and their derivatives are smooth in a close neighborhood ( $r^* - \epsilon, r^* + \epsilon$ ) of  $r^*$  ( $\epsilon \ll \Delta$ ) during the collapsing process. This implies the following (almost unique) way to implement the boundary condition : The interface is modeled by three points  $r^* \pm \Delta$  and  $r^*$ , where  $\Delta$  is now the grid spacing. Both  $\delta P$  and  $\delta T$  *as well as* their derivatives are continuous at  $r^*$ , while the values of  $\delta P$  and  $\delta T$  at  $r^* + \Delta$  and  $r^* - \Delta$  are determined by their solutions inside and outside  $r^*$ . Thus, if sharp changes ever occur in the solution, they will only occur at  $r^* \pm \Delta$  and nowhere else.

As we shall see in **A** below, our numerical method reproduces a set of non-trivial modes which and can also be obtained analytically. These modes exist in each angular momentum sector and are *independent of the validity of LDA*. The fact that our calculations reproduce the exact results for each  $\ell$  shows that the boundary conditions have been implemented correctly [11].

**Main Results** : Because of spherical symmetry,  $\delta P$  and  $\delta T$  can be resolved into spherical harmonic components  $(\delta P(\mathbf{r}), \delta T(\mathbf{r})) = \sum_{\ell, n, m} (\delta P_{\ell n}(r), \delta T_{\ell n}(r)) Y_{\ell m}(\hat{\mathbf{r}})$ , where  $\ell$  is the angular momentum and  $n$  is the radial quantum number. Each  $(\ell, n)$  mode is  $2\ell + 1$  fold degenerate. We have performed calculations for  $^{87}\text{Rb}$  ( $a = 58.2\text{\AA}$ ) for the number of trapped atoms  $N$  varying from  $N = 10^4$  to  $10^8$ . The general features of all these systems are identical. For concreteness, we present the results for  $N = 10^6$  particles in a trap, with  $\omega_T/2\pi = 200\text{Hz}$ , over the range  $0.6 < T/T_c < 1.2$  where Eqs.(9) and (10) are valid. Our solutions reveal two kinds of modes which are the analogs of the first and second sound modes in homogenous systems :

**(A) First sound** : These modes exist both above and below  $T_c$ . They are *in phase* pressure and temperature oscillations that extend over the entire cloud, and  $\delta P$  has one more node than  $\delta T$ . The frequencies of these modes (denoted as  $\omega_{\ell n_1}^{(1)}$ ) are shown in Fig.1 for  $\ell = 0, 1, 2$  and  $n_1 = 0$  to 4, where  $n_1$  counts the number of nodes of  $\delta P$  in the radial direction. While the frequencies change with temperature, their variations are small compared to  $\omega_T$ . The eigenfunctions of the  $(\ell = 1, n_1 = 2)$  mode at  $T = 0.84T_{co}$  are shown in Fig.2a. They extend over the entire cloud. This feature is common to all first sound modes above and below  $T_c$ .

The  $n_1 = 0$  modes are special. They are isothermal modes of the form

$$\delta P(r, \hat{\mathbf{r}}) = n_o(r) r^\ell Y_{\ell m}(\hat{\mathbf{r}}), \quad \delta T = 0, \quad \text{with} \quad \omega_{\ell, 0}^{(1)} = \omega_T \sqrt{\ell}. \quad (11)$$

They are also “universal” in the sense that they are *independent of interaction and statistics*. *These results emerge from our numerical solution* but can be obtained analytically from Eqs.(5) and (7) . With  $\delta T = 0$ , using the equilibrium relations given by Eq.(2), Eqs.(5) and (7) can be shown to yield

$$\nabla^2(\delta P/n_o) = 0, \quad \text{and} \quad \partial_t^2(\delta P/n_o) = -\nabla \phi \cdot \nabla(\delta P/n_o). \quad (12)$$

The form of  $\delta P$  given in Eq.(11) is a solution to the above equations. From Eqs.(3) to Eq.(6), it is straightforward to show that  $\mathbf{v}_n = \mathbf{v}_s$  below  $T_c$ , and that  $\nabla \cdot \mathbf{v}_n = 0$  both above and below  $T_c$ .

The  $(\ell = 0, n_1 = 1)$  mode is also special. Above  $T_c$ , it is a uniform temperature oscillation,  $\nabla \delta T = 0$ , but with  $\delta T \neq 0$ . This mode is “non-universal” because it depends on interactions. The interaction effect, however, is sufficiently weak so that  $\omega_{0,1}^{(1)}$  is very close to  $2\omega_T$  above  $T_c$ . It is also straightforward to show that  $\nabla \cdot \mathbf{v}_n$  is constant but nonzero for this mode. These results can be established analytically using LDA and also emerge as part of our numerical solutions. Below  $T_c$ ,  $\delta T$  is no longer uniform, and  $\nabla \cdot \mathbf{v}_n$  is not a constant [12]. All the other sound modes  $(\ell, n_1 \neq 0)$  are non-isothermal.

**(B) Second Sound :** These modes only exist below  $T_c$ . The frequencies of these modes for  $(\ell = 0, 1, 2)$  and  $(n_2 = 0, 1, 2)$  are shown in Fig.1. *It should be stressed that the second sound frequencies do not merge into the first sound frequencies as  $T \rightarrow T_c$ .* To illustrate this clearly, we plot  $\omega_{\ell, n_2=1}^{(2)}$  near  $T_c$  (for  $\ell = 0$  to 2) as a function of particle number  $N$  in Fig.3. While  $\omega_{\ell, n_2=1}^{(2)}$  changes with  $N$ , the first sound frequencies (not shown in Fig.3) typically vary by about 2% of  $\omega_T$  in the same range of  $N$ . The eigenfunctions of the  $(\ell = 1, n_2 = 2)$  mode are shown in Fig.2b. An enlarged structure of the interface of this mode at  $r^*$  is shown in Fig.2c. These eigenmodes have the following features that are common to all second sound modes :

(1) The pressure ( $\delta P$ ) and temperature ( $\delta T$ ) oscillations are “out of phase” inside the condensate and become “in phase” as they leak out into the normal region. The leakage reduces to zero as  $T \rightarrow T_c$ . The quantum number  $n_2$  counts the number of nodes of  $\delta P$  or  $\delta T$  inside the condensate.

(2) The wavelengths of the oscillations shrink as  $r \rightarrow r^*$ . This can be understood simply from LDA by recalling that the second sound velocity  $c_2$  of a homogenous dilute Bose gas is proportional to  $\sqrt{n_{so}}$ . The wavelength  $k^{-1}$  of a second sound with frequency  $\omega$  is therefore  $k^{-1} = c_2/\omega \propto \sqrt{n_{so}}$ . Since  $\omega \sim \omega_T$  in our case, and  $n_{so}(r)$  vanishes as  $r \rightarrow r^*$ , so will the local wavelength  $k^{-1}(r)$ .

(3) In terms of dimensionless quantities  $[\delta \tilde{P}, \delta \tilde{T}] \equiv [\delta P/(n_o(\mathbf{r})k_B T_o), \delta T/T_o]$ , we find that  $\delta \tilde{T}/\delta \tilde{P} \gg 1$  as  $T \rightarrow T_c$ . In comparison,  $\delta \tilde{P} \sim \delta \tilde{T}$  for the first sound mode near  $T_c$ .

(4) In  $^4\text{He}$ , the normal and superfluid currents in the second sound mode almost cancel each other, *i.e.*,  $\xi \equiv |n_n v_n / n_s v_s| \sim 1$ . However, plotting  $\xi$  obtained from our solution as a function of  $r$ , we find that in addition to the vanishing and diverging behaviors near the nodes of  $v_n$  and  $v_s$ , the typical value of  $\xi$  is about 0.3. This result can again be understood in terms of LDA. From the work of Lee and Yang [13], one finds that  $\xi = \frac{12}{5}(a/\lambda)(g_{3/2}^2(1)/g_{5/2}(1))$  for the homogenous dilute Bose gas, which is around 0.3 for the temperature range studied [14].

**Comparison with the JILA data:** Examining the JILA data [5] on the sound modes of  $^{87}\text{Rb}$  with  $\sim 2 \times 10^3$  atoms, we find surprising consistencies with the behavior of the sound modes of larger systems that we studied.

**(a)** An  $(m = 0)$  mode with frequency  $\approx 2\omega_T$  was observed for all  $T$  above  $T_c$  [5]. The analog of this mode in a spherical trap is the  $(\ell = 0, n_1 = 1)$  first sound mode, which also has frequency  $\approx 2\omega_T$  for all  $T$  above  $T_c$ .

**(b)** Below  $T_c$ , the frequency of the  $(m = 0)$  mode falls from about  $2\omega_T$  to  $1.85\omega_T$  as  $T$  decreases from  $0.9T_{co}$  to  $0.5T_{co}$  [5]. The first and second sound analogs of this mode below  $T_c$  are the  $(\ell = 0, n_1 = 1)$  and the  $(\ell = 0, n_2 = 1)$  modes respectively. The observed behavior

matches well with the ( $\ell = 0, n_2 = 1$ ) second sound mode, which drops from about  $1.9\omega_T$  to  $1.5\omega_T$  as  $T$  decreases from  $0.8T_{co}$  to  $0.6T_{co}$  as seen from Fig.1.

(c) An ( $m = 2$ ) mode was also observed below  $T_c$  [5]. Its frequency decreases from  $1.45\omega_T$  to  $1.25\omega_T$  as  $T$  increases from  $0.5T_{co}$  to  $0.85T_{co}$ . The second sound analog of this mode in spherical trap is the ( $\ell = 2, n_2 = 0$ ) mode, which also drops from about  $1.4\omega_T$  to about  $1.35\omega_T$  as  $T$  increases from  $0.5T_{co}$  to  $0.85T_{co}$ .

While we do not expect perfect agreement of our results with the JILA observations [5] because of the difference in trap symmetry and particle numbers, the qualitative and quantitative consistencies over the temperature and angular momentum range mentioned above are striking. The above discussions suggest that the ( $m = 0$ ) and ( $m = 2$ ) modes observed below  $T_c$  [5] are both second sound modes. It is not clear at present why the first sound modes do not appear with great prominence below  $T_c$ . Whether it is due to the way that the modes are excited or due to the fact that density oscillations below  $T_c$  might contain a large second sound component because of the large temperature fluctuations in the second sound modes (as mentioned in Discussion (3) above) will be studied later. To clearly identify the nature of the sound modes, it is necessary to experimentally investigate larger number of modes so as to have more consistency checks with the hydrodynamic predictions. We hope that this work will stimulate and provide guidance for future experiments.

VBS would like to thank Allan McLeod for providing the programs on  $g_\nu$ , and Vijay Shenoy and Shiwei Zhang for discussions on numerical methods. Various parts of this work were performed during TLH's regular visits to CalTech during Winter and Spring of 97. He would specially like to thank M.C. Cross for hospitality. This work is supported by NSF Grant No. DMR-9705295.

## REFERENCES

- [1] M.H. Anderson, J.R. Ensher, M.R. Mathews, C.E. Weiman, and E.A. Cornell, *Science* **269**, 198 (1995). C.C. Bradley, C.A. Sackett, J.J. Tollett, and R.G. Hulet, *Phys. Rev. Lett.* **75**, 1687 (1995). K.B. Davis, M.O. Mewes, M.R. Andrews, N.J. van Druten, D.S. Durfee, D.M. Kurn, and W. Ketterle, *Phys. Rev. Lett.* **75**, 3969 (1995).
- [2] G. Baym and C.J. Pethick, *Phys. Rev. Lett.* **76**, 6 (1996). M. Edwards and K. Burnett, *Phys. Rev. A* **51**, 1382 (1995).
- [3] M.-O. Mewes, *et al.*, *Phys. Rev. Lett.* **77**, 988 (1996). D.S. Jin, *et al.*, *Phys. Rev. Lett.* **77**, 420 (1996).
- [4] S. Stringari, *Phys. Rev. Lett.* **77**, 1405 (1996).
- [5] D.S. Jin, M.R. Matthews, J.R. Ensher, C.E. Weiman and E.A. Cornell, *Phys. Rev. Lett.* **78**, 764 (1997).
- [6] G.M. Kavoulakis, C.J. Pethick, and H. Smith, (cond-mat/9710130) have recently pointed out that for the parameters of the Colorado trap about  $10^7$  atoms are required to attain the hydrodynamic limit near  $T_c$ .
- [7] See for example, Chap.I, Sec.4 of S.J. Putterman, *Superfluid Hydrodynamics*, North Holland, 1974. The hydrodynamic equations for single component and binary mixtures of Bose gas in external potentials have been derived in great detail in T.L. Ho and V.B. Shenoy, submitted to JLTP.
- [8] T.T. Chou, C.N. Yang and L.H. Yu, *Phys. Rev. A* **53**, 4257 (1996).
- [9] See Fig.7 of S. Giorgini, L.P. Pitaevskii, S. Stringari, cond-mat/9704014.
- [10] T.D. Lee and C.N. Yang, *Phys. Rev.* **112**, 1419 (1958).
- [11] Another problem which has similar feature is the collective mode equation for the density deviation  $\delta\rho$  in Thomas-Fermi approximation, where the density  $\rho_0$  vanishes at  $r = R$  with a discontinuous slope, see (Stringari, *ibid*). Realizing that this abrupt change in slope occurs as a result of collapsing the actual interface into a surface, we can implement the boundary conditions for  $\delta\rho$  in a manner similar to the one adopted in this paper. We have solved the collective mode equation with these boundary condition and have recovered all the analytic results of Stringari (Stringari. *ibid*), which once again shows the correctness of our method.
- [12] Both types of special modes ( $\ell \neq 0, n_1 = 0$ ) and ( $\ell = 1, n_1 = 1$ ) were also found by A.Griffin *et al.*, *Phys. Rev. Lett.* **78**, 1838 (1997) in a study of the hydrodynamics of trapped ideal Bose gas above  $T_c$ . Interaction effects and the way these modes extend below  $T_c$  were however not investigated.
- [13] T.D. Lee and C.N. Yang, *Phys. Rev.* **6**, 1406 (1959).
- [14] Our results contradict the conjecture of E. Zaremba *et al.*, (cond-mat/9705134) that the second sound oscillations satisfy  $n_n \mathbf{v}_n + n_s \mathbf{v}_s \approx 0$  like  $^4\text{He}$ .



**Figure 1:** Temperature dependence of the first and second sound frequencies ( $\omega_{\ell n_1}^{(1)}$  and  $\omega_{\ell n_2}^{(2)}$ ) for  $\ell = 0, 1$  and 2 in units of trap frequency  $\omega_T$  for  $10^6$   $^{87}\text{Rb}$  atoms in a spherical trap with  $\omega_T = 1256.6 \text{sec}^{-1}$  (200Hz). The open and filled symbols represent the first and second sound modes respectively. For each  $\ell$ , the first sound modes are classified by the quantum number  $n_1$  specifying the number of nodes in  $\delta P$ , while the second sound modes are classified by the number of nodes  $n_2$  of  $\delta P$  or  $\delta T$  inside the superfluid region. For the modes with  $\ell \neq 0$ ,  $r = 0$  is not counted as a node. The dotted line at  $0.917T_{co}$  indicates the critical temperature  $T_c$  of the interacting model, where  $T_{co}$  is the condensation temperature of the ideal Bose gas in the trap. We have plotted temperatures in units of  $T_{co}$  in order to facilitate comparison with the JILA experimental results. The eigenmodes of first and second sound modes marked A and B (at  $0.84T_{co}$ ) are shown in Fig.2.

**Figure 2a:** The pressure and temperature oscillations of the first sound mode ( $\ell = 1, n_1 = 2$ ) marked as A in Fig.1 is plotted as functions of radial distance measured in units of oscillator width  $a_T$ . The dashed vertical line (at  $r = r^*$ ) separates the superfluid and normal regions. The label  $n_1 = 2$  for the first sound modes specifies the number of nodes in pressure oscillations; pressure oscillations have one more node than the temperature oscillations. The oscillations  $\delta P$  and  $\delta T$  are “in phase” in both the superfluid and normal regions. To magnify the features, we have multiplied  $\delta P$  and  $\delta T$  by  $r^2$ . (This is a phase space factor typical in evaluating quantities per unit radial distance).

**Figure 2b:** The pressure and temperature oscillations of the second sound mode ( $\ell = 1, n_2 = 2$ ) marked as B in Fig.1 is plotted as functions of radial distance measured in units of oscillator width  $a_T$ . The label  $n_2 = 2$  for the second sound mode denotes the the number of nodes in the pressure or temperature oscillations inside the superfluid region. The oscillations  $\delta P$  and  $\delta T$  are “out of phase” inside the condensate but “in phase” in the normal region. No  $r^2$  factor such as that in Fig.2a is multiplied to  $\delta P$  and  $\delta T$  of this mode because their features are sufficiently clear.

**Figure 2c:** The detailed structure of the superfluid-normal interface of the second sound mode in Fig.2(b). The filled point indicates the exact location of the interface. The grid spacing in this region is  $\Delta = 0.005a_T$ . The sharp change of slope at the interface of the superfluid and the normal regions is expected as our boundary condition is meant to simulate the collapsing process of LDA at  $r^*$ . (Details can be found in our discussions on *Numerical Methods*).

**Figure 3:** The frequency of the second sound modes ( $\ell, n_2 = 1$ ) in the vicinity of  $T_c$  versus particle number  $N$ . The figure shows the modes with  $\ell = 0, 1, 2$  for  $N$  varying between  $10^4$  and  $10^8$ . The temperature is chosen so that the radius of the superfluid droplet  $r^*$  is equal to the trap width  $a_T$ .

**Fig.1**

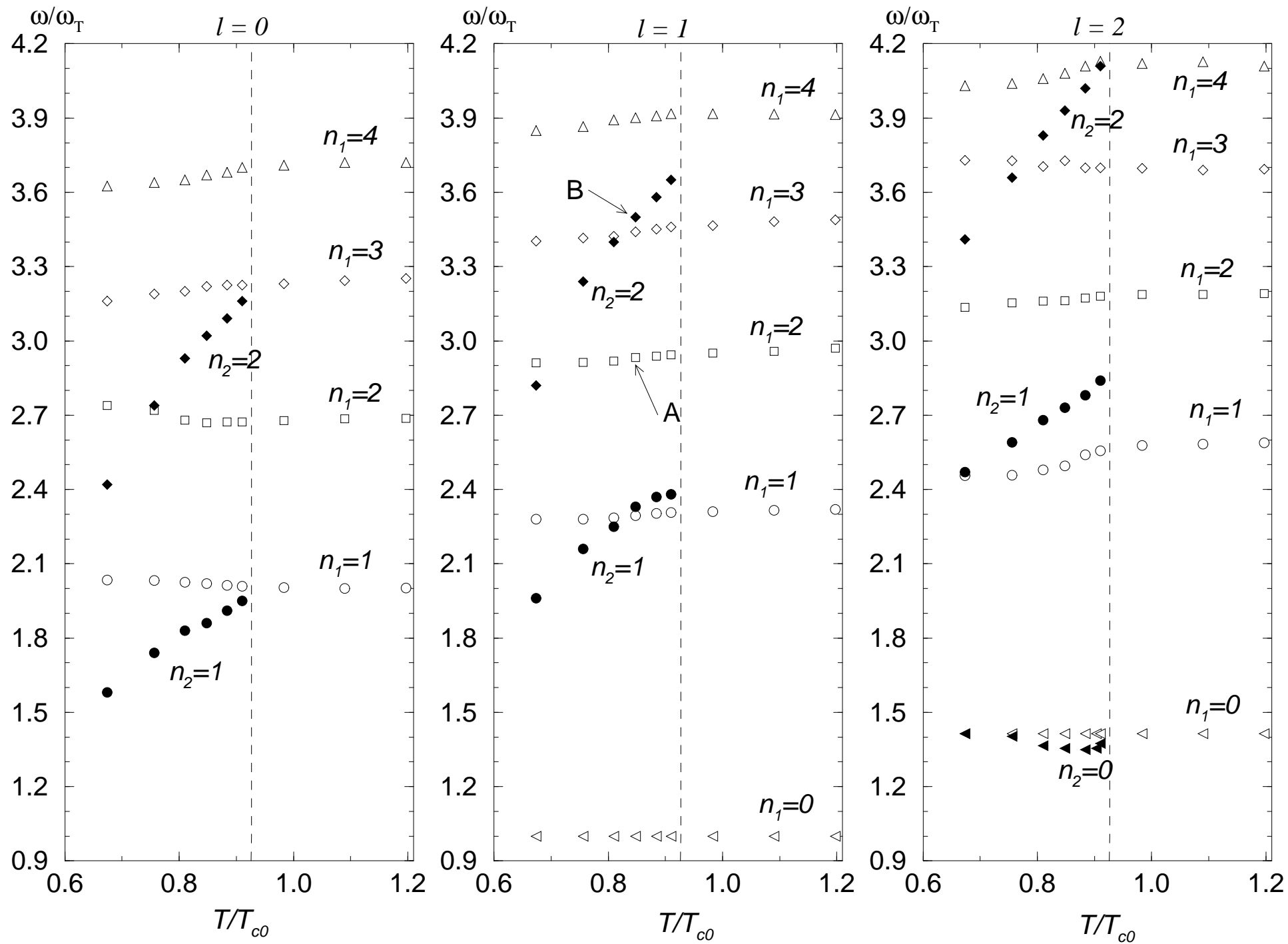


Fig.2(a)

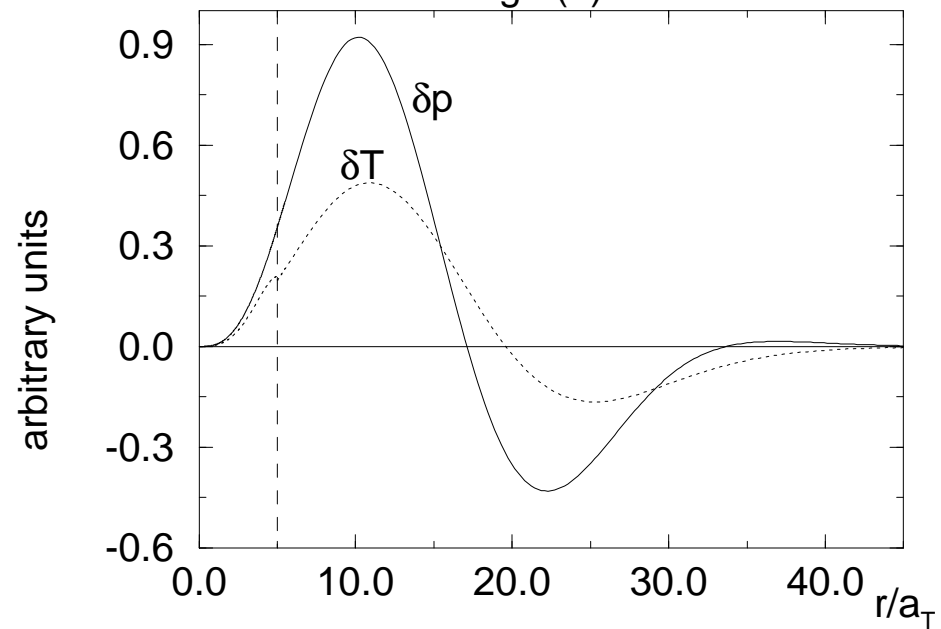


Fig.2(b)

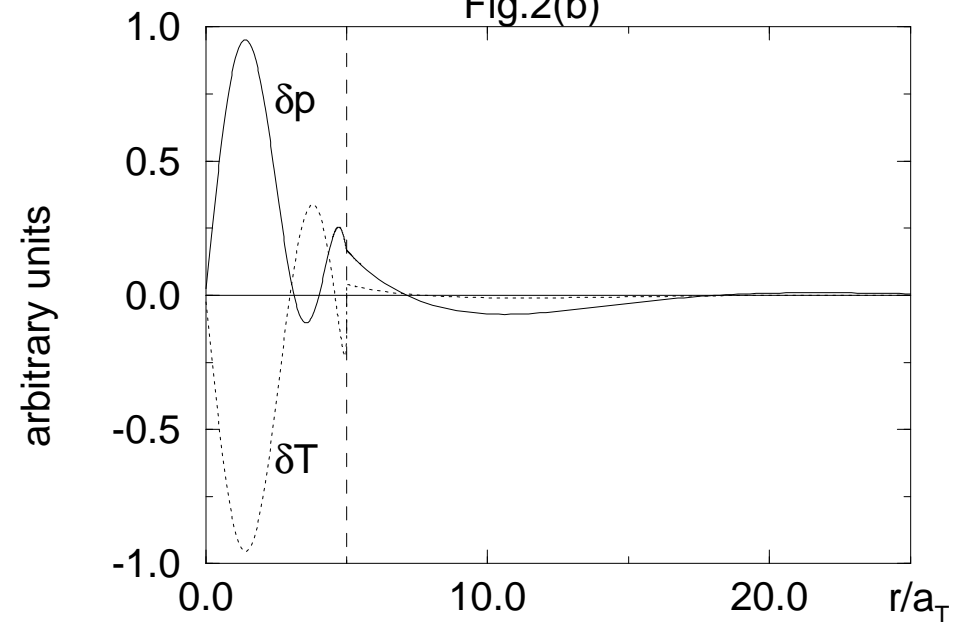


Fig.2(c)

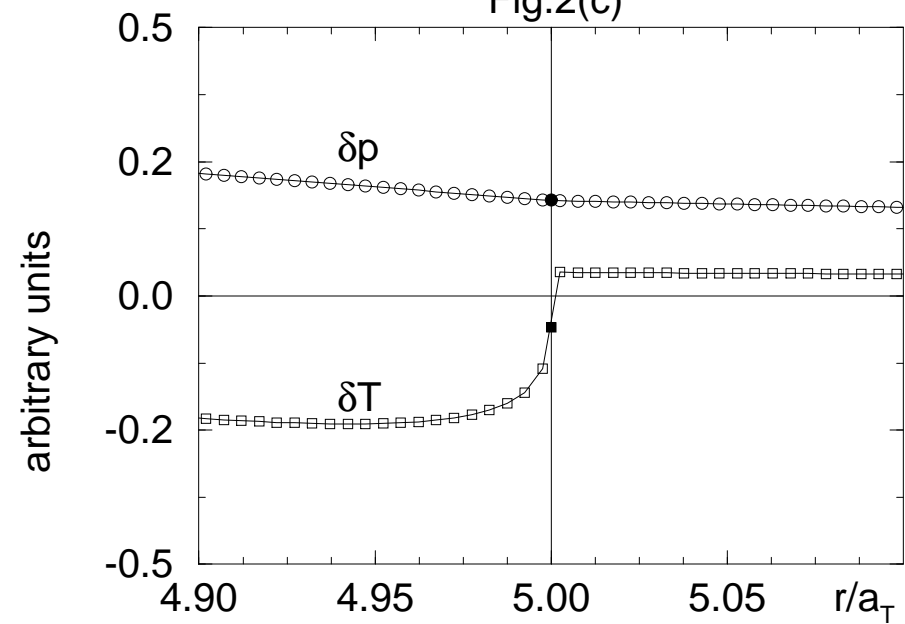


Fig.3

